THE ROYAL SOCIETY

Wavelets for the study of intermittency and its topology

By F. Nicolleau† and J. C. Vassilicos

Department of Applied Mathematics and Theoretical Physics, University of Cambridge, Silver Street, Cambridge CB3 9EW, UK

We make a distinction between two topologically different types of intermittency: isolated, as in spirals, and non-isolated, as in fractals. For a broad class of isolated and a broad class of non-isolated intermittent topologies, the flatness $F(r)$ of velocity differences and the eddy capacity D_{E} obtained from a wavelet analysis are related by

$$F(r) \sim r^{D_{\mathrm{E}}-1}.$$

Inertial range intermittency is such that $D_{\mathrm{E}} \leqslant 0.94$ and $F(r) \sim r^{-0.11}$ for jet turbulence with $Re_\lambda = 835$ and for grid turbulence with $Re_\lambda = 3050$.

Keywords: fractals; spirals; singularities; intermittency; wavelets; turbulence

1. Introduction

The intermittency of a statistically homogeneous signal $u(x)$ is often characterized by the flatness (Batchelor 1953; Frisch 1995),

$$F(r) = \frac{\langle \Delta u^4(r) \rangle}{\langle \Delta u^2(r) \rangle^2}, \tag{1.1}$$

where $\Delta u(r) = u(x+r) - u(x)$, the brackets $\langle \dots \rangle$ denote an average over x. A signal is often said to be intermittent when $F(r)$ increases with decreasing r. This is because an intermittent signal displays activity (in the sense that Δu is significantly non-zero) over only a fraction of space (or time) x, and this portion decreases with the scale r under consideration. However, such a property does not shed much light on the actual topology of the signal's intermittency. In this paper we use the wavelet transform to study what intermittency can actually look like in space, how we can measure its geometry, and we introduce a distinction between two different topologies of intermittency.

These different topologies can give rise to the same flatness properties. When the signal $u(x)$ is statistically scale invariant, then we may talk of scale-invariant intermittency and $F(r)$ must have a power-law dependence on r, i.e.

$$F(r) \sim r^{-q}. \tag{1.2}$$

This power q is a global statistical quantity, but we show that it is determined by the local geometry of the intermittency of the signal. The geometry of a signal and

† Present address: Department of Mechanical Engineering, University of Sheffield, Mappin Street, Sheffield S1 3JD, UK.

the degree to which this geometry is space filling are usually studied in terms of Kolmogorov capacities (fractal or box dimensions) of zero-crossings of the signal. However, we show here that the geometry of the *intermittency* of the signal is best captured by the zero-crossings of the *second derivative* of the signal, and that the Kolmogorov capacity of these zero-crossings can determine q.

2. Intermittency and eddy capacity

The zero-crossings of the second derivative $(\mathrm{d}^2/\mathrm{d}x^2)u(x)$ are related to both the geometry and the statistics of the intermittency of the signal $u(x)$. The signal $u(x)$ being assumed statistically homogeneous, nth-order moments $\langle|\Delta u(r)|^n\rangle$ can, therefore, be calculated as follows (see Frisch 1995):

$$\langle|\Delta u(r)|^n\rangle = \lim_{T\to\infty}\frac{1}{T}\int_0^T |u(x+r)-u(x)|^n\,\mathrm{d}x. \tag{2.1}$$

In the limit where $r\to 0$, $\Delta u(r)=u(x+r)-u(x)$ is extremal at inflection points of the signal $u(x)$, that is, at points where $(\mathrm{d}^2/\mathrm{d}x^2)u(x)=0$. In those cases where $|\Delta u(x)|$ has the same order of magnitude at all these inflection points, we can estimate that

$$\langle|\Delta u(r)|^n\rangle \sim |\Delta u(r)|^n r M_{\mathrm{E}}(r), \tag{2.2}$$

where $M_{\mathrm{E}}(r)$ is the minimum number of segments of size r needed to cover the zero-crossings of $(\mathrm{d}^2/\mathrm{d}x^2)u(x)$ per unit length. If the signal $u(x)$ is statistically scale invariant, then $M_{\mathrm{E}}(r)$ has a power-law dependence on r, and this power-law dependence defines the eddy capacity D_{E} as follows:

$$M_{\mathrm{E}}(r)\sim r^{-D_{\mathrm{E}}}. \tag{2.3}$$

Hence, D_{E} is the Kolmogorov capacity of the zero-crossings of $(\mathrm{d}^2/\mathrm{d}x^2)u(x)$, and note that $0\leqslant D_{\mathrm{E}}\leqslant 1$. From (2.2) and (2.3),

$$\langle|\Delta u(r)|^n\rangle \sim |\Delta u(r)|^n r^{1-D_{\mathrm{E}}},$$

and the r dependence of non-dimensionalized structure functions is given by

$$\frac{\langle|\Delta u(r)|^n\rangle}{\langle|\Delta u(r)|^2\rangle^{n/2}} \sim r^{(1-D_{\mathrm{E}})(1-(n/2))}. \tag{2.4}$$

For $n=4$ we obtain

$$F(r)\sim r^{D_{\mathrm{E}}-1}, \tag{2.5}$$

and a comparison of (2.5) with (1.2) gives

$$q = 1-D_{\mathrm{E}}. \tag{2.6}$$

These conclusions are similar to the results of the β-model,

$$\frac{\langle|\Delta u(r)|^n\rangle}{\langle\Delta u^2(r)\rangle^{n/2}} \sim r^{(1-D)(1-(n/2))},$$

where D is a fractal dimension defined in terms of the volume fraction $p(r)$ of eddies of size r (see Frisch 1995). However, in the β model, the concept of an eddy of size

r remains abstract and no operative definition is given by which to identify and measure an eddy of size r.

In this respect, the situation is radically different here. An operative definition is given by which to measure D_{E} in terms of accessible properties of the signal, the inflection points of the signal. These properties are indirectly accessible in practice if use is made of a wavelet transform,

$$\tilde{u}(x_0, a) = a^{-3} \int u(x)\psi^* \left(\frac{x - x_0}{a} \right) \mathrm{d}x, \tag{2.7}$$

of the signal $u(x)$, where $\psi(x)$ is the 'mother' wavelet (ψ^* its complex conjugate). The first relatively minor advantage in using a wavelet transform is of avoiding calculation of double derivatives of the signal. This is explained in the next paragraph. The second major advantage in using a wavelet transform is that it can provide an estimate of the importance of the drop in $u(x)$ at scale r across the inflection point. This is explained in conclusion (v) in § 3.

The wavelet transform is a function of position x_0 and length-scale a. Choosing the mother wavelet in (2.7) to be a Mexican hat, that is

$$\psi(x) = \frac{\mathrm{d}^2}{\mathrm{d}x^2} \mathrm{e}^{-x^2/2},$$

the zeros of $\tilde{u}(x_0, a)$ tend towards zeros of $(\mathrm{d}^2/\mathrm{d}x^2)u(x_0)$ as $a \to 0$. Hence, the eddy capacity D_{E} can be measured in practice as follows: a Mexican hat wavelet transform $\tilde{u}(x_0, a)$ is performed on the signal $u(x)$ and a box-counting algorithm is applied on the zero-crossings of $\tilde{u}(x_0, a)$ for the smallest scale a permitted by the discretization. The box counting yields $M_{\mathrm{E}}(r)$ and an eddy capacity is well defined if $M_{\mathrm{E}}(r) \sim r^{-D_{\mathrm{E}}}$ over a significant range of scales. This wavelet-box-counting algorithm to measure D_{E} is applied successfully in the following section to test the validity of $F(r) \sim r^{D_{\mathrm{E}}-1}$ against a variety of test signals. We have checked in all cases that the value of D_{E} can be obtained unchanged from the zero-crossings of $\tilde{u}(x_0, a)$ for many values of a even larger than the discretization.

In this paper, we restrict ourselves to the study of scale-invariant intermittency for which $D_{\mathrm{E}} > 0$. (See the appendix for a short discussion of the differences between D_{E} and the Kolmogorov capacity D'_{K} of the zero-crossings of the signal $u(x)$ itself.)

3. Validity of $F(r) \sim r^{D_{\mathrm{E}}-1}$

Hunt & Vassilicos (1991) emphasize that signals with power spectra $E(k) \sim k^{-2p}$, where $p < 1$ (such as Kolmogorov's $k^{-5/3}$), must contain singularities (or rather near-singularities if we take into account small-scale smoothing effects such as those of viscosity or diffusivity) that are worse than mere isolated discontinuities in the signal or its derivatives. These singularities can be qualitatively classified as follows (Hunt & Vassilicos 1991): isolated cusp singularities such as $1/x$; isolated accumulating singularities such as $\sin(1/x)$ (see figures 4*b* and 5); and non-isolated singularities such as can be found in fractal signals (see figures 1, 4*a*, 7*a* and 8*b*). Simple models of small-scale turbulence structure have been proposed for each one of these singularities: the Burgers vortex (see Batchelor 1967) has a point vortex near-singularity that is a cusp near-singularity; the Lundgren vortex (Lundgren 1982) has a spiral-vortex-sheet near-singularity that is an isolated accumulating near-singularity; and fractal

and multifractal models of turbulence, such as the β model and its generalizations (see Frisch 1995), assume the existence of non-isolated singularities.

We test the validity of (2.5) numerically on several model signals $u(x)$, some regular and others scale invariant, with qualitatively different types of singularity. The conclusions are outlined below.

(i) *For continuous signals with continuous derivatives, for signals with isolated discontinuities in the signal itself or its derivatives, and for isolated cusps,* $D_{\mathrm{E}} = 0$ *and* $F(r) = \text{const.}$

This conclusion implies that signals in which $D_{\mathrm{E}} \neq 0$ or $F(r) \neq \text{const.}$ must necessarily have either isolated accumulating singularities or non-isolated singularities, thus leading to a topological classification of intermittency for which $D_{\mathrm{E}} \neq 0$: *isolated intermittency* when the intermittent signal carries isolated accumulating singularities but no non-isolated singularities; and *non-isolated intermittency* when the intermittent signal carries non-isolated singularities.

It should be noted, however, that isolated accumulating singularities with $D_{\mathrm{E}} = 0$ and $F(r) = \text{const.}$ are possible, e.g. $u(x) = \sin(\mathrm{e}^{1/x})$, and that non-isolated singularities with $D_{\mathrm{E}} = 0$ are also possible.

(ii) *For fractal signals with* $F(r) = \text{const.}$, $D_{\mathrm{E}} = 1$ *irrespective of the power spectrum's scaling.*

There exists a class of fractal signals (non-isolated singularities) for which

$$F(r) = \text{const.} \quad \text{and} \quad D_{\mathrm{E}} = 1,$$

irrespective of their power spectrum's scaling, $E(k) \sim k^{-2p}$. Examples of such fractal signals are the Weierstrass function,

$$u(x) = \sum_{j \geqslant 1} \lambda^{(\alpha-2)j} \sin(\lambda^j x), \tag{3.1}$$

where $\lambda > 1$ and $1 < \alpha < 2$ (figure 1*a*); the random-phase fractal signal obtained by replacing $\sin(\lambda^j x)$ with $\sin(\lambda^j x + \phi_j)$ in (3.1), where ϕ_j is a random phase between 0 and 2π (figure 1*b*); and the sum of centred sinusoids,

$$u(x) = \sum_{j \geqslant 1} \lambda^{(\alpha-2)j} \sin(\lambda j \pi x), \tag{3.2}$$

where λ is an integer and $1 < \alpha < 2$ (figure 1*c*). For all these signals, and irrespective of the values of λ and α that determine the power spectrum (see Falconer 1990), we find that $D_{\mathrm{E}} = 1$ and $F(r) = \text{const.}$ (figure 2).

(iii) *However, there exist signals with non-isolated singularities for which* $F(r) \sim r^{-q}$ *but* $D_{\mathrm{E}} = 1$.

This is the case of the function $u(x)$ defined in Benzi *et al.* (1993) (see figure 3) as

$$u(x) = \sum_{j=0}^{15} \sum_{k=0}^{2^j-1} \alpha_{i,j} \Psi(2^j x - k), \tag{3.3}$$

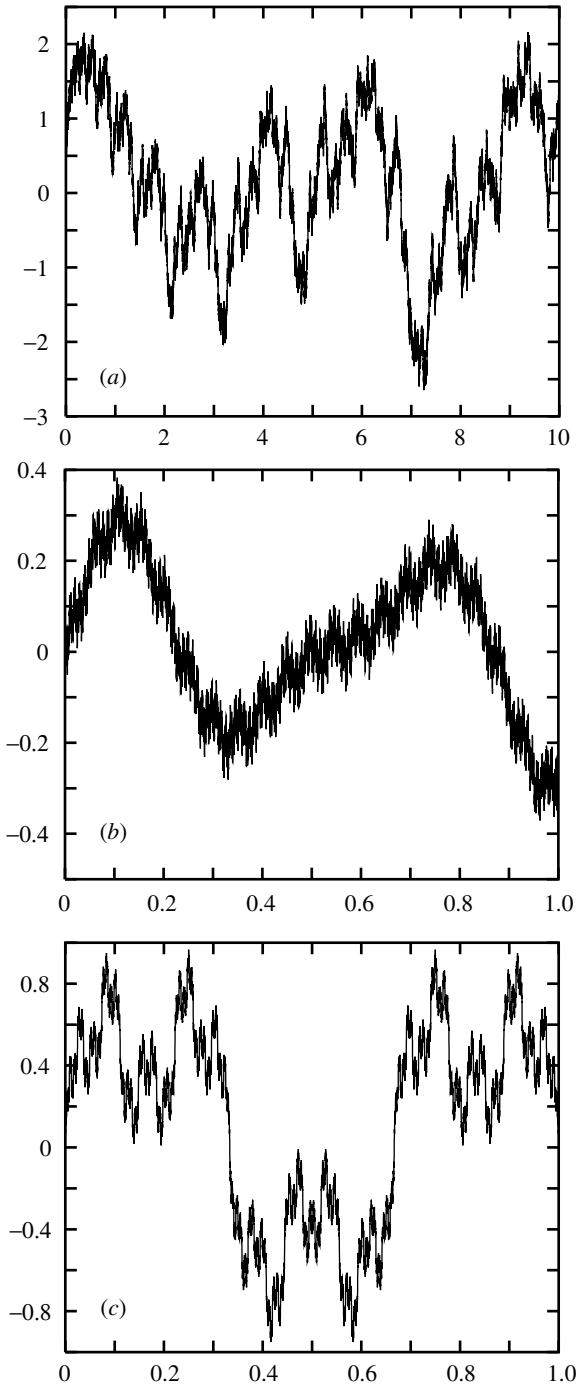

Figure 1. Non-intermittent signals. (*a*) The Weierstrass function (3.1) (here $\lambda = \alpha = 1.5$ and $j \leqslant 30$). (*b*) The random-phase function (here $\lambda = \alpha = 1.5$ and $j \leqslant 30$). (*c*) The centred sinusoid function (3.2) (here $\lambda = 3$, $\alpha = 1.5$ and $j \leqslant 25$). These are signals with non-isolated singularities and are such that $D_{\mathrm{E}} = 1$ (see figure 2).

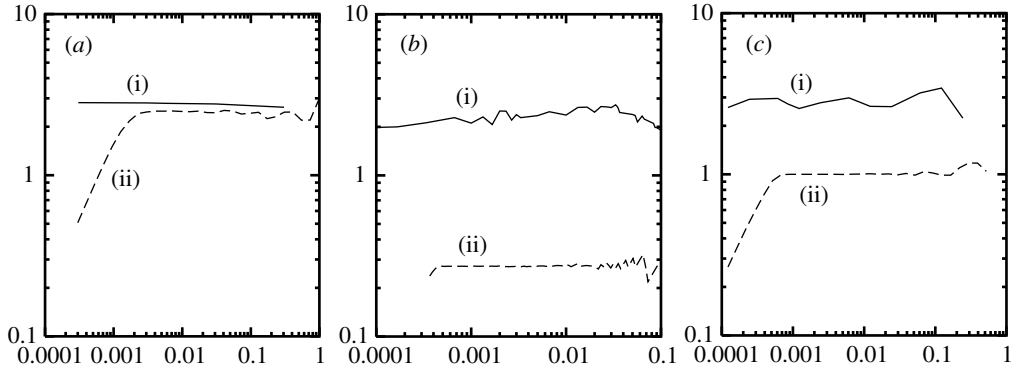

Figure 2. Comparison of (i) $r^{D_{\mathrm{E}}}M_{\mathrm{E}}(r)$ and (ii) $r^{1-D_{\mathrm{E}}}F(r)$ as functions of r; $M_{\mathrm{E}}(r)$ is the minimum number of segments of size r needed to cover the zero-crossings of $(\mathrm{d}^2/\mathrm{d}x^2)u(x)$ per unit length. (a) Weierstrass function; (b) random-phase function; (c) centred sinusoid function. We have set $D_{\mathrm{E}} = 1$ in all these graphs to demonstrate that $D_{\mathrm{E}} = 1$ in all the cases presented in figure 1.

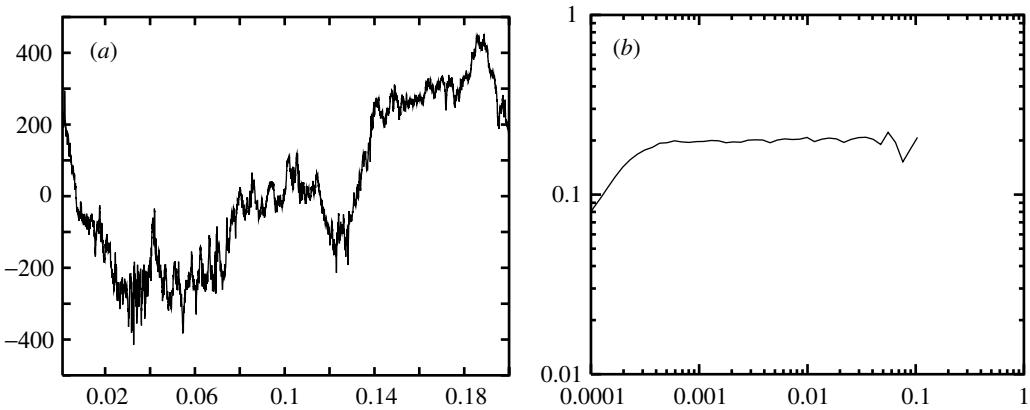

Figure 3. (a) Function with non-isolated singularities defined by (3.3), for which $F(r) \sim r^{-0.27}$ but $D_{\mathrm{E}} = 1$. The probability density function of η is $P(\eta) = y\eta_0 + (1-y)\eta_1$ with $y = 0.2924$, $\eta_0 = 0.70$, $\eta_1 = 0.45$, $\sigma = 0.18$. (b) Plot of $r^{D_{\mathrm{E}}}M_{\mathrm{E}}(r)$ against r for this function, where we have set $D_{\mathrm{E}} = 1$.

where

$$\Psi(x) = -\frac{\partial^2}{\partial x^2}\mathrm{e}^{-(x^2)/(2\sigma^2)}, \qquad \alpha_{j,k} = \epsilon_{j,k}\eta_{j,k}\alpha_{j-1,k/2},$$

the $\eta_{j,k}$ are independent random variables and $\epsilon_{j,k} = \pm 1$ with equal probability. For this function $u(x)$, there exist sets of random variables $\eta_{i,j}$ for which $F(r) \sim r^{-q}$ with $q \neq 0$ (Benzi *et al.* 1993), but we invariably find that $D_{\mathrm{E}} = 1$.

(iv) *If D_{E} is well defined and $D_{\mathrm{E}} < 1$ and if $F(r) = r^{-q}$, then $q = 1 - D_{\mathrm{E}}$ for a broad class of isolated and a broad class of non-isolated intermittent topologies.*

Let us start with the restricted class of on–off signals, such as those pictured in figure 4. These signals take one of two values, say -1 and $+1$. They can have either

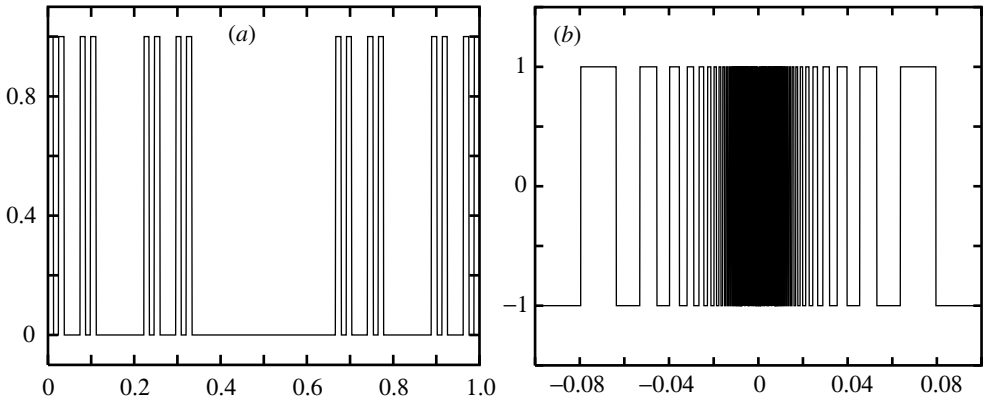

Figure 4. Intermittent signals with non-isolated (a) and isolated (b) singularities. (a) The Cantor dust on–off function (here, $D'_{\mathrm{K}} = D_{\mathrm{E}} = \ln 2/\ln 3$). ($b$) On–off signal (3.4) (here, $D'_{\mathrm{K}} = D_{\mathrm{E}} = \frac{1}{3}$).

isolated intermittency, as in the function

$$u(x) = H(\sin(x^{-t})) - H(-\sin(x^{-t})) \tag{3.4}$$

(figure 4b), where H is the Heaviside function, or non-isolated intermittency as in the well-known Cantor set (figure 4a). When the set of points where the signal abruptly changes value is characterized by a well-defined Kolmogorov capacity D'_{K}, the flatness

$$F(r) \sim r^{D'_{\mathrm{K}}-1}.$$

This result has been derived analytically by Vassilicos (1992) for on–off signals with either isolated accumulating singularities or non-isolated singularities. On–off signals are such that $D_{\mathrm{E}} = D'_{\mathrm{K}}$ because the zero-crossings of the second derivatives of such signals are the same as the zero-crossings of the signal itself. It is therefore an analytical result† that for on–off signals with either isolated or non-isolated intermittency:

$$F(r) \sim r^{D_{\mathrm{E}}-1}.$$

For these on–off signals, the assumption made in (2.2), that $|\Delta u(x)|$ has the same order of magnitude at all the inflection points, is indeed verified. However, we find that $F(r) \sim r^{D_{\mathrm{E}}-1}$ is valid even beyond this assumption. The following numerical examples demonstrate that $F(r) \sim r^{D_{\mathrm{E}}-1}$ is valid more generally when $|\Delta u(x)|$ does not have too strong a dependence on x, in the cases of both isolated and non-isolated intermittency.

An example of a family of signals with isolated intermittency for which this assumption is not verified (unless $s = 0$) is (see figure 5a–c)

$$u(x) = x^s \sin(x^{-t}). \tag{3.5}$$

The Fourier power spectrum is well defined when $-1 \leqslant 2s \leqslant t$ and $t > 0$. For these signals, $F(r) \sim r^{-q}$ and $q = 1 - D_{\mathrm{E}}$ (figure 6a, b) provided that $-1 \leqslant 2s \leqslant t$ and $t > 0$. However, if the cusp singularity superimposed onto the isolated accumulation is too strong, that is if s is too negative (i.e. if $2s < -1$) as in the example of figure 5c, then $q \neq 1 - D_{\mathrm{E}}$ (figure 6c).

† More generally, the analytical results of Vassilicos (1992) imply that (2.4) holds for all values of n when the signal is on–off.

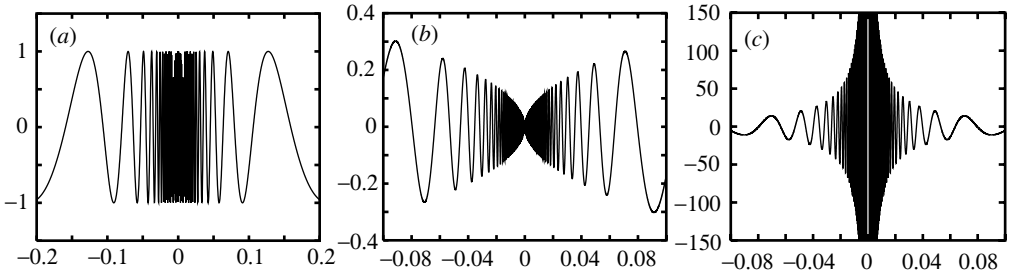

Figure 5. Isolated intermittency for different spiral functions: (*a*) $\sin x^{-1/2}$ ($D'_{\mathrm{K}} = D_{\mathrm{E}} = \frac{1}{3}$); (*b*) $x^{1/2} \sin x^{-1}$ ($D'_{\mathrm{K}} = D_{\mathrm{E}} = \frac{1}{2}$); (*c*) $x^{-1} \sin x^{-1}$ ($D'_{\mathrm{K}} = 0.5$, $D_{\mathrm{E}} = 0.6$).

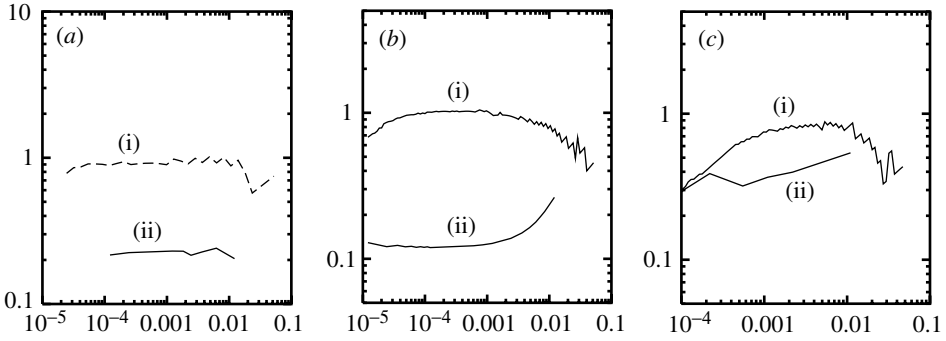

Figure 6. Comparison of (i) $r^{D_{\mathrm{E}}} M_{\mathrm{E}}(r)$ and (ii) $r^{1-D_{\mathrm{E}}} F(r)$ as functions of r, for the signals with isolated intermittency of figure 5. (*a*) The function $\sin x^{-1/2}$ (we set $D_{\mathrm{E}} = \frac{1}{3}$). (*b*) The function $x^{1/2} \sin x^{-1}$, (we set $D_{\mathrm{E}} = \frac{1}{2}$). (*c*) The function $x^{-1} \sin x^{-1}$ (we set $D_{\mathrm{E}} = 0.6$) and the absence of plateaux indicates here that $F(r) \sim r^{D_{\mathrm{E}}-1}$ is not valid. The plateaux in (*a*), (*b*) indicate that $F(r) \sim r^{D_{\mathrm{E}}-1}$ is valid for these functions.

The non-isolated intermittency of figure 7*a* is constructed on the basis of a Cantor set of points of Kolmogorov capacity D'_{K} but differently: the value of the signal between two consecutive such points is l^{σ}, where l is the distance between these two points and σ is a real number. This is also a signal where $|\Delta u(x)|$ depends on x. Nevertheless, $F(r) \sim r^{D_{\mathrm{E}}-1}$ is valid for this signal too (figure 7*b*) provided that $\sigma > -\frac{1}{2}$.

However, there exist examples of isolated and non-isolated intermittency where $F(r) \sim r^{D_{\mathrm{E}}-1}$ is not valid even for arbitrarily weak dependencies of $|\Delta u(x)|$ on x. This is the case for the isolated intermittencies of figures 5*c* and 8*a*, and for the non-isolated intermittency of figure 8*b*. The signal of figure 8*a* is based on the zero-crossings of signals (3.4) and (3.5), which are given by $x_n = (n\pi)^{-1/t}$, n being a positive integer. This signal (figure 8*a*) is defined as follows:

$$u(x) = \sum_{n \geqslant 1} (l_n)^{\sigma} H(x - x_{n+1}) H(x_n - x), \tag{3.6}$$

where $l_n = x_n - x_{n+1}$ and σ is a real number. For such signals, $F(r) \sim r^{-q}$ but $q \neq 1 - D_{\mathrm{E}}$, irrespective of the value of σ. Furthermore, figure 8*b* is a Devil's staircase constructed on a Cantor set of points of Kolmogorov capacity D'_{K} (see, for

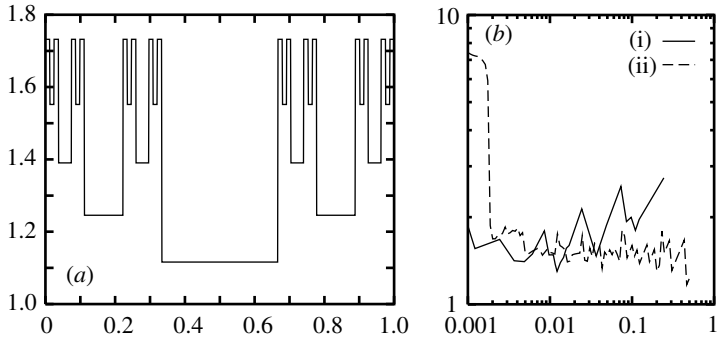

Figure 7. (*a*) The non-isolated intermittent signal described in conclusion (iii) (here, $\sigma = 0.25$ and $D_{\mathrm{E}} = 0.7$). (*b*) (i) $r^{1-D_{\mathrm{E}}}F(r)$ and (ii) $r^{D_{\mathrm{E}}}M_{\mathrm{E}}(r)$ for this signal; the ratio of the largest to the smallest scale is 6500. $F(r) \sim r^{D_{\mathrm{E}}-1}$ is verified, but, due to the properties of lacunarity of this signal, $r^{1-D_{\mathrm{E}}}F(r)$ exhibits strong oscillations. $r^{D_{\mathrm{E}}}M_{\mathrm{E}}(r)$ keeps its plateau shape on the large scales, whereas $r^{1-D_{\mathrm{E}}}F(r)$ loses its precision on these scales.

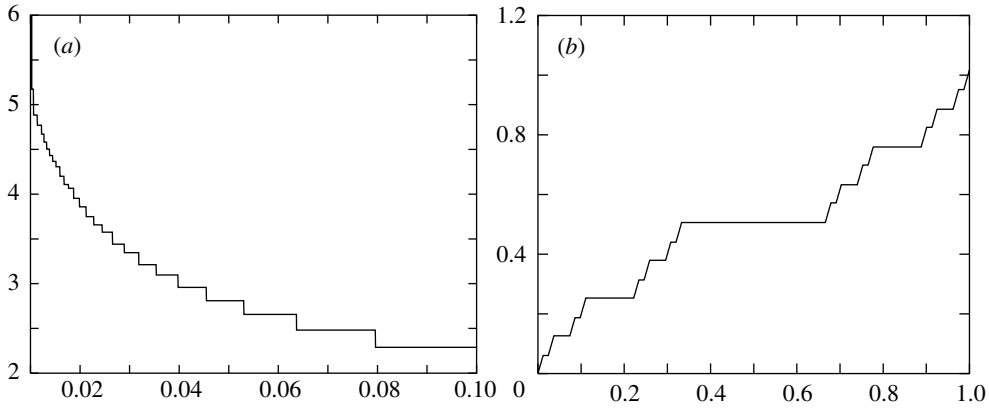

Figure 8. Different signals with isolated (*a*) and non-isolated (*b*) intermittency for which $F(r) \sim r^{D^*_{\mathrm{E}}-1}$ is verified but $F(r) \sim r^{D_{\mathrm{E}}-1}$ is not verified. (*a*) Stair function (3.6) based on the zero-crossings of $\sin x^{-1}$ (here, $D^*_{\mathrm{E}} = 0.65$, $\sigma = 0.2$). (*b*) Devil's staircase (here, $D^*_{\mathrm{E}} = 0.7$ with 2000 for the ratio of the largest to the smallest scale).

example, Frisch 1995), and for this case of non-isolated intermittency, we also find that $F(r) \sim r^{-q}$, but $q \neq 1 - D_{\mathrm{E}}$.

The definition of D_{E} can be refined in such a way that $q = 1 - D_{\mathrm{E}}$ can be made valid for these last two types of signals too.

(v) *The definition of D_{E} can be refined using additional information from wavelet transforms to extend the domain of validity of $F(r) \sim r^{D_{\mathrm{E}}-1}$.*

The wavelet transform $\tilde{u}(x_0, a)$ of the signal $u(x)$ is

$$\tilde{u}(x_0, a) = a^{-3} \int u(x)\psi^*\left(\frac{x - x_0}{a}\right) \mathrm{d}x,$$

and if the 'mother' wavelet is a Mexican hat, that is if

$$\psi(x) = \frac{\mathrm{d}^2}{\mathrm{d}x^2}\mathrm{e}^{-x^2/2},$$

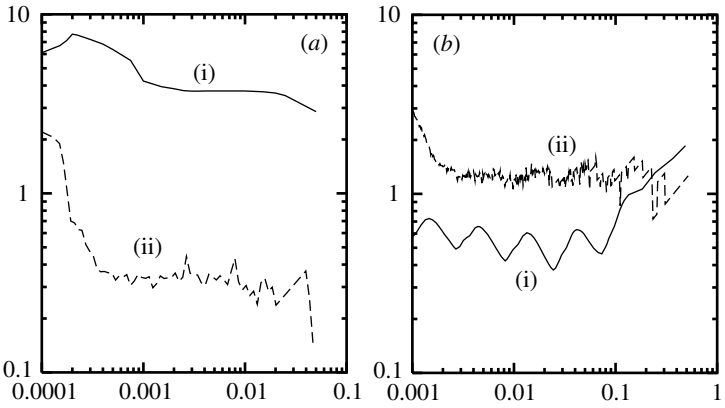

Figure 9. Plots of (i) $r^{1-D_{\mathrm{E}}^*}F(r)$ and (ii) $r^{D_{\mathrm{E}}^*}M_{\mathrm{E}}(r)$ as functions of r. (a) Case 8a (we set $D_{\mathrm{E}}^* = 0.65$). (b) Devil's staircase with a scale ratio of 2000 (we set $D_{\mathrm{E}}^* = 0.7$). $F(r) \sim r^{D_{\mathrm{E}}^*-1}$ is verified for both cases, but, for the signal in figure 8b, $r^{1-D_{\mathrm{E}}^*}F(r)$ exhibits strong oscillations due to the properties of lacunarity of this signal; note that in this case $r^{D_{\mathrm{E}}^*}M_{\mathrm{E}}(r)$ keeps its plateau shape on the large scales, whereas $r^{1-D_{\mathrm{E}}^*}F(r)$ loses its precision on these scales.

then the zeros of $\tilde{u}(x_0, a)$ tend towards zeros of $(\mathrm{d}^2/\mathrm{d}x^2)u(x_0)$ as $a \to 0$. Zero-crossing curves of $\tilde{u}(x_0, a)$ in the x_0–a plane start at a point $(x_0', a_{\max})$, and, as a is decreased towards $a = 0$, end at a point $(x_{\mathrm{I}}, 0)$, where $(\mathrm{d}^2/\mathrm{d}x^2)u(x_{\mathrm{I}}) = 0$. Hence, a characteristic length-scale $a_{\max}$ is assigned to every inflection point x_{I}, and it is therefore possible to define turbulent eddies that are positioned at x_{I} and that have a size and intensity related to $a_{\max}$ (see Kevlahan & Vassilicos 1994). The minimum number $M_{\mathrm{E}}^*(r)$ of segments of size r needed to cover the inflection points x_{I} with $a_{\max} \geqslant r$ (this sole condition differentiates $M_{\mathrm{E}}^*(r)$ from $M_{\mathrm{E}}(r)$) gives a measure of the number of eddies of size larger than r, and an eddy capacity D_{E}^* can be defined if the signal is self-similar, in which case

$$M_{\mathrm{E}}^*(r) \sim r^{-D_{\mathrm{E}}^*}. \tag{3.7}$$

Clearly, $M_{\mathrm{E}}^*(r) \leqslant M_{\mathrm{E}}(r)$. Furthermore, there can exist no inflection point x_{I} for which $a_{\max} = 0$. This is because zero-crossings of $\tilde{u}(x_0, a)$ tend towards *all* zero-crossings of $(\mathrm{d}^2/\mathrm{d}x^2)u(x_0)$ as $a \to 0$, and, therefore, if an inflection point x_{I} existed for which $a_{\max} = 0$, this inflection point could not be approached continuously by zeros of $\tilde{u}(x_0, a)$ as $a \to 0$. Hence, there exists a minimum value of $a_{\max}$, which we call $a_{\min}$, and which is different from zero. Noting that

$$\begin{aligned} M_{\mathrm{E}}^*(a_{\min}) &= M_{\mathrm{E}}(a_{\min}), \\ M_{\mathrm{E}}^*(r) &= M_{\mathrm{E}}^*(a_{\min})(r/a_{\min})^{-D_{\mathrm{E}}^*}, \\ M_{\mathrm{E}}(r) &= M_{\mathrm{E}}(a_{\min})(r/a_{\min})^{-D_{\mathrm{E}}}, \end{aligned}$$

we obtain

$$(r/a_{\min})^{-D_{\mathrm{E}}^*} \leqslant (r/a_{\min})^{-D_{\mathrm{E}}}, \tag{3.8}$$

for $r/a_{\min} \geqslant 1$, and we therefore conclude that

$$D_{\mathrm{E}}^* \geqslant D_{\mathrm{E}}. \tag{3.9}$$

Table 1. *Different eddy capacities and flatness factors of the signals in figures 1, 4, 5, 7a, 8 and 12*

(D_{E} is the Kolmogorov capacity of the zero-crossings of $(\mathrm{d}^2/\mathrm{d}x^2)u(x)$; D_{E}^* is computed using the refined definition (3.7) based on the wavelet transform (2.7).)

figure	type	D_{E}^*	D_{E}	$F(r)$
1*a*	non-isolated	1	1	$r^{D_{\mathrm{E}}-1} \sim 3$
1*b*	non-isolated	1	1	$r^{D_{\mathrm{E}}-1} \sim 2$
1*c*	non-isolated	1	1	$r^{D_{\mathrm{E}}-1} \sim 3$
4*a*	non-isolated	0.63	0.63	$6 \neq r^{D_{\mathrm{E}}-1}$
5*c*	non-isolated	0.6	0.5	$r^{1/6} \neq r^{D_{\mathrm{E}}-1}$
3*a*	non-isolated	1	1	$r^{-0.27}$
5*a*	isolated	0.33	0.33	$r^{D_{\mathrm{E}}-1}$
5*b*	isolated	0.50	0.50	$r^{D_{\mathrm{E}}-1}$
4*b*	isolated	0.33	0.33	$r^{D_{\mathrm{E}}-1}$
8*a*	isolated	0.65	0.5	$r^{D_{\mathrm{E}}^*-1}$
7*a*	non-isolated	0.7	0.63	$r^{D_{\mathrm{E}}^*-1}$
8*b*	non-isolated	0.7	0.7	$r^{D_{\mathrm{E}}-1}$
12*a*	jet	0.92	—	$r^{-0.11}$
12*b*	wind-tunnel	0.95	—	$r^{-0.11}$

D_{E}^* is a refined definition of an eddy capacity, which, unlike D_{E}, takes into account the intensity of $|\Delta u|$ at inflection points x_{I} in such a way that

$$F(r) \sim r^{D_{\mathrm{E}}^*-1}$$

is valid over a wider class of signals than

$$F(r) \sim r^{D_{\mathrm{E}}-1}.$$

In particular, we find numerically that $D_{\mathrm{E}}^* = D_{\mathrm{E}}$ in all the cases where we find that $q = 1 - D_{\mathrm{E}}$ (see table 1). For signals of type (3.6) (figure 8*a*) and for the Devil's staircase (figure 8*b*), $D_{\mathrm{E}}^* > D_{\mathrm{E}}$ and $q = 1 - D_{\mathrm{E}}^*$, whereas $q \neq 1 - D_{\mathrm{E}}$ (see figure 9).

In the remainder of this paper (including figures), the eddy capacity is invariably defined in terms of the more refined wavelet algorithm giving D_{E}^*, which is in fact a very practical tool for computing the eddy capacity, and we replace the notation D_{E}^* by D_{E} for the sake of simplicity.

(vi) *In the absence of noise, D_{E} is a better measure of intermittency than $F(r)$.*

Our conclusions (iv) and (v) can be summarized with the statement that $F(r) \sim r^{D_{\mathrm{E}}-1}$ for a broad class of isolated and non-isolated intermittent topologies.

We now find that D_{E} is a better *measure* of intermittency than $F(r)$ in the absence of noise. We deal with the problem of noise in § 4.

In all the model signals in which we find that $F(r) \sim r^{D_{\mathrm{E}}-1}$, D_{E} appears to be a more sensitive measure of intermittency than $F(r)$ in two respects. Firstly, the measurement of D_{E} only requires a well-resolved, but relatively small, part of the signal, whereas $F(r)$ needs large amounts of data to converge. Secondly, $F(r)$ is

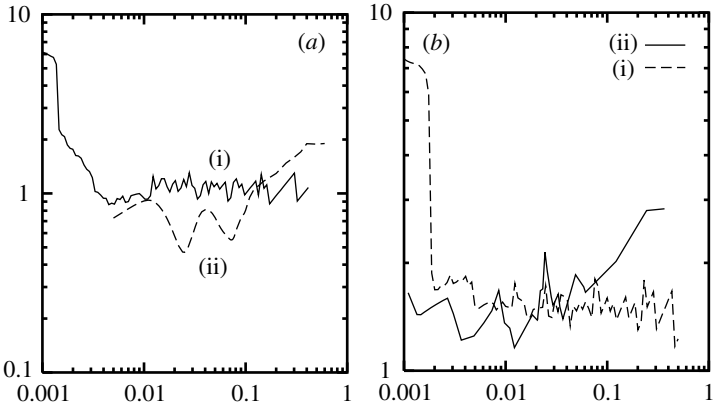

Figure 10. Comparison of the accuracy of D_{E} and $F(r)$. (a) Devil's staircase with a ratio of scales of only 81 ($D_{\mathrm{E}} = 0.7$). (b) Case 7a with a ratio of scales of only 2000 ($D_{\mathrm{E}} = 0.7$). (i) $r^{D_{\mathrm{E}}} M(r)$ keeps its plateau shape in both (a) and (b), whereas (ii) $r^{1-D_{\mathrm{E}}} F(r)$ exhibits no plateau slope in (a) and does but on a very limited range of scales in (b).

more sensitive than D_{E} to the outer cut-off scale of the self-similar range and can exhibit oscillations (Smith *et al.* 1986). In all our model signals, D_{E} remains well defined and accurate even close to the outer cut-off scale, whereas $F(r)$ does not. This means that $F(r)$ needs a larger self-similar range of scales than D_{E} to ensure a good accuracy on the measurement of the power law. Typically, the ratio of the outer cut-off (sampling size) to the inner cut-off (resolution) needs to be of the order of 10–100 for an accurate measurement of D_{E}. Whereas, a ratio of 100 is not enough for the dependence of $F(r)$ on r to reach its asymptotic form. This is particularly clear in the comparison of figures 7b, 9b and 10, which display the measurement of D_{E} and $F(r)$ for the signals of figures 7a and 8b. These two signals are fractal constructions, and a fractal resolution is defined by the ratio of the outer cut-off to the inner cut-off scales of the fractal process. The highest resolution is that of figures 7b and 9b, and the smallest that of figure 10 (see figure captions for details), and it turns out that D_{E} is accurately measured and well defined for both resolutions, whereas the r dependence of $F(r)$ is closer to its asymptotic form only in the cases of figures 7b and 9b, where the resolution is best.

Particularly striking are the cases of some fractal on–off signals where we know that $F(r) \sim r^{D_{\mathrm{E}}-1}$ analytically (see figure 4a). The numerical results obtained for various resolutions indicate that $F(r)$ does not exhibit, in practice, its asymptotic form $r^{D_{\mathrm{E}}-1}$ unless the resolution is really extraordinary. Nevertheless, D_{E} is always well defined even for low resolutions of the fractal on–off structure, and is found, as expected, to be equal to D'_{K}, the Kolmogorov capacity of the set of points where the signal changes values. Of course, this class of intermittent signals is extreme in that these signals are equal to, say, zero nearly everywhere except on a fractal set (a Cantor set in the case of figure 4a). Nevertheless, D_{E} can capture the intermittency even in such extreme situations, whereas $F(r)$ cannot do so except if the resolution is enormous (see figure 11a).

Hence, in the absence of noise, as is the case of all our model signals, D_{E} requires smaller datasets and smaller self-similar ranges than $F(r)$ to be determined accurately. However, in the presence of even a small amount of noise, a direct measure-

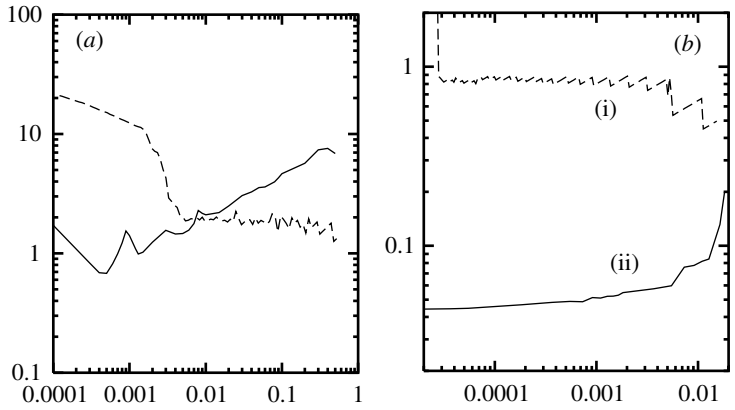

Figure 11. Plots of $r^{D_E} M_E(r)$ (dashed line) and $r^{1-D_E} F(r)$ (solid line) as functions of r for the two signals in figure 4. (a) Cantor dust on–off function, $D_E = 0.63$. (b) On–off spiral signal, $D_E = \frac{1}{3}$; the plateau is observed, indicating that $F(r) \sim r^{D_E - 1}$.

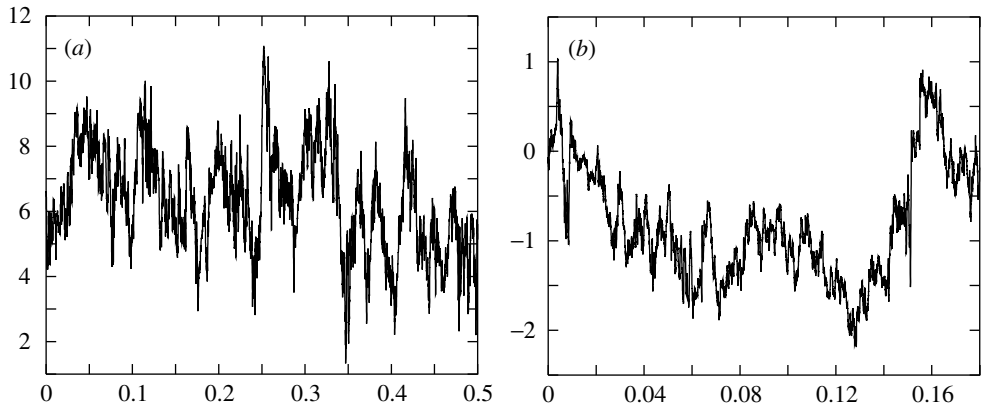

Figure 12. Experimental one-point turbulent velocity signals from Modane. u against time. (a) Jet turbulent velocity. (b) Wind-tunnel turbulent velocity (see table 2.)

ment of D_E gives $D_E = 1$ irrespective of the underlying intermittent structure onto which the noise is superimposed (Kevlahan & Vassilicos 1994). In the following section, we show how to make D_E robust to the presence of noise, and we measure the eddy capacity D_E and flatness $F(r)$ of the two one-point turbulent velocity signals of figure 12.

4. Application to high resolution turbulent velocity signals

Signals measured in practice always contain some noise strongly affecting their eddy-capacity measurement. To deal with this problem, we propose to replace the direct measure of the eddy capacity on the measured signal $u_{\mathrm{meas}}(x)$ by a measure on a 'distilled' signal $u_J(x)$ extracted from the measured signal. Our aim is to discard in this intermediary signal $u_J(x)$ the effect of noise and retrieve part of the structure of the underlying signal $u(x)$ (that is the ideal physical signal without noise). To construct this intermediary signal, we start by defining a series of increasing thresh-

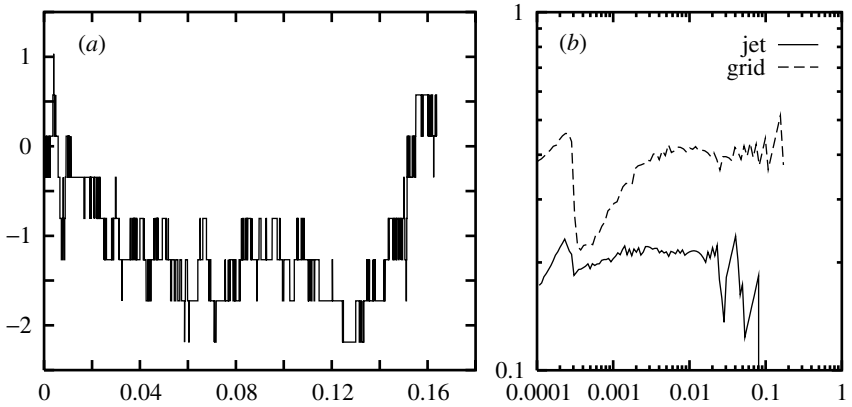

Figure 13. (*a*) $u_J(x)$ in case 12*b* with $J = 8$, based on the 8192 first points that correspond to $0 < x < 0.114$. (*b*) $r^{D_E} M_E(r)$ measured on figure 12*a*, *b* with $J = 8$, as functions of r, $D_E = 0.95$.

olds $U_0, U_1, U_2, \ldots, U_J$ evenly spaced between the minimum and maximum values ($u_{\min}$ and $u_{\max}$) of the measured signal $u_{\text{meas}}(x)$ ($U_j = u_{\min} + j[(u_{\max} - u_{\min})/J]$ for $j = 0, \ldots, J$). The points x_i, where $u_{\text{meas}}(x_i)$ equals one of these thresholds, say $u_{\text{meas}}(x_i) = U_j$, are given in increasing order ($x_i < x_{i+1}$) and so that $u_{\text{meas}}(x_{i+1})$ equals either U_{j+1} or U_{j-1}. The intermediary signal is defined as follows:

$$u_J(x) = \sum_{i \leqslant J} u_{\text{meas}}(x_i)(H(x - x_i) - H(x - x_{i+1})). \tag{4.1}$$

Figure 13*a* shows this construction for the experimental signal of figure 12*b* with $J = 7$.

The measured signal $u_{\text{meas}}(x)$ results from the superimposition of noise on $u(x)$. We may express this noise in the form $\epsilon(x)u(x)$, where $\epsilon(x)$ is a dimensionless random function of x, in which case

$$u_{\text{meas}}(x) = u(x)(1 + \epsilon(x)). \tag{4.2}$$

We can then compute the quantity $M_E(r)$ both for the measured signal $u_{\text{meas}}(x)$ and for each intermediary signal $u_J(x)$, and from now on we restrict the notation $M_E(r)$ to the signal without noise $u(x)$ and use $M_E^{\text{meas}}(r)$ and $M_E^J(r)$ for, respectively, the measured signal $u_{\text{meas}}(x)$ and the intermediary signal $u_J(x)$. The construction of the intermediary signals introduces a new scale $r_{\min}^J = \min(|x_{i+1} - x_1|)$, below which $u_J(x)$ contains no information about $u_{\text{meas}}(x)$. Hence, any measurement's noise below $r_{\min}^J$ is not in $u_J(x)$. The computation of $M_E^J(r)$ is based on the algorithm introduced in conclusion (v) of § 3, for which only zero-crossing curves (in the x_0–a plane) of $\tilde{u}_J(x_0, a)$ with $a_{\max} > r$ are counted in $M_E^J(r)$. Any zero-crossing curves of $\tilde{u}_{\text{meas}}(x_0, a)$ caused by noise and such that $a_{\max} < r_{\min}^J$, are, therefore, eliminated from the calculation of $M_E^J(r)$ for $r > r_{\min}^J$. One may expect that the remaining zero-crossing curves that are taken into account in the calculation of $M_E^J(r)$ are those of $\tilde{u}_{\text{meas}}(x_0, a)$ with $a_{\max} \geqslant r > r_{\min}^J$, along with a few extra zero-crossing curves introduced by the discontinuous nature of the construction of $u_J(x)$ itself. But we conjecture that for sufficiently large $r_{\min}^J$, that is sufficiently small J, the procedure by which we construct $u_J(x)$ effectively removes noise even at scales larger than $r_{\min}^J$,

so that the zero-crossing curves that are counted in the calculation of $M_{\mathrm{E}}^{J}(r)$ are in fact those of $\tilde{u}(x_0, a)$ with $a_{\max} \geqslant r > r_{\min}^{J}$, along with the extra zero-crossing curves introduced by the construction of $u_J(x)$. On this basis we can write

$$M_{\mathrm{E}}(r) \leqslant M_{\mathrm{E}}^{J}(r) \leqslant M_{\mathrm{meas}}(r),$$

for $r > r_{\min}^{J}$, and we may conclude that where eddy capacities are well defined,

$$D_{\mathrm{E}} \leqslant D_{\mathrm{E}}^{J} \leqslant D_{\mathrm{E}}^{\mathrm{meas}},$$

with obvious notation. To validate the above conjecture, we verify the inequality

$$D_{\mathrm{E}} \leqslant D_{\mathrm{E}}^{J} \leqslant D_{\mathrm{E}}^{\mathrm{meas}},$$

on three different types of signals, each with a different singularity structure: fractal (figure 14*a*), spiral (figure 14*c*) and spirals on a fractal set (figure 14*e*). We also verify on these signals that where D_{E}^{J} is constant over a range of J, then $D_{\mathrm{E}} = D_{\mathrm{E}}^{J}$ for these values of J, and where D_{E}^{J} is not constant for a range of J, $D_{\mathrm{E}} < D_{\mathrm{E}}^{J}$. Finally, we also verify that the maximum value of J for which $D_{\mathrm{E}}^{J} \leqslant D_{\mathrm{E}}^{\mathrm{meas}}$ may be expected to hold is determined by the requirement that $U_j \epsilon_{\max} < U_{j+1} - U_j$ for all j, which implies that

$$J < [(u_{\max} - u_{\min})/u_{\max]\epsilon_{\max}}$$

(assuming that a maximum value $\epsilon_{\max}$ exists such that $\epsilon_{\max} \geqslant |\epsilon(x)|$). Of course, it is also necessary that $1 \leqslant J$ for $u_J(x)$ not to be trivial.

The left-hand plots of figure 14 show the signals with some added noise corresponding to $\epsilon_{\max} = 0.1$ (current experimental hot-wire probes have a typical accuracy of the order of 1%). Figure 14*a* corresponds to the case of figure 7*a*, figure 14*c* to a spiral accumulation with $D'_{\mathrm{K}} = 0.5$, and figure 14*e* to a compounded signal obtained by placing spiral accumulations on a Cantor set. In the right-hand plots of figure 14, we report measurements of D_{E}^{J}, $D_{\mathrm{E}}^{\mathrm{meas}}$ against D_{E}. Specifically, in figure 14*b*, *d*, *f*, we plot $r^{D_{\mathrm{E}}} M_{\mathrm{E}}(r)$, $r^{D_{\mathrm{E}}} M_{\mathrm{E}}^{J}(r)$ and $r^{D_{\mathrm{E}}} M_{\mathrm{E}}^{\mathrm{meas}}(r)$. The lowest curves in these right-hand plots correspond to $r^{D_{\mathrm{E}}} M_{\mathrm{E}}(r)$ (no noise), the uppermost curves to $r^{D_{\mathrm{E}}} M_{\mathrm{E}}^{\mathrm{meas}}(r)$, and intermediate curves with intermediate slopes to $r^{D_{\mathrm{E}}} M_{\mathrm{E}}^{J}(r)$. Note that in all the cases of figure 14, the value of $r^{D_{\mathrm{E}}} M_{\mathrm{E}}^{J}(r)$ is, at the largest scales, the same for all

$$J < [(u_{\max} - u_{\min})/(u_{\max}\epsilon_{\max})].$$

This observation supports the claim that the extra zero-crossings in the wavelet plane introduced by the very construction of $u_J(x)$ do not affect the r dependence of $M_{\mathrm{E}}^{J}(r)$ for $r > r_{\min}^{J}$. In figure 14*b*, we plot $r^{D_{\mathrm{E}}} M_{\mathrm{E}}^{J}(r)$ for the signal in figure 14*a* for different values of J. In this case,

$$[(u_{\max} - u_{\min})/(u_{\max}\epsilon)] = 3.7,$$

and, indeed, a loss in precision is observed for $J > 3$. The signal without noise has an eddy capacity $D_{\mathrm{E}} = 0.7$, whereas, due to the noise, the signal of figure 14*a* has an eddy capacity equal to 1. In figure 14*f*, we plot $r^{D_{\mathrm{E}}} M_{\mathrm{E}}^{J}(r)$ corresponding to figure 14*e* for different values of J. In this example,

$$[(u_{\max} - u_{\min})/(u_{\max}\epsilon_{\max})] = 20,$$

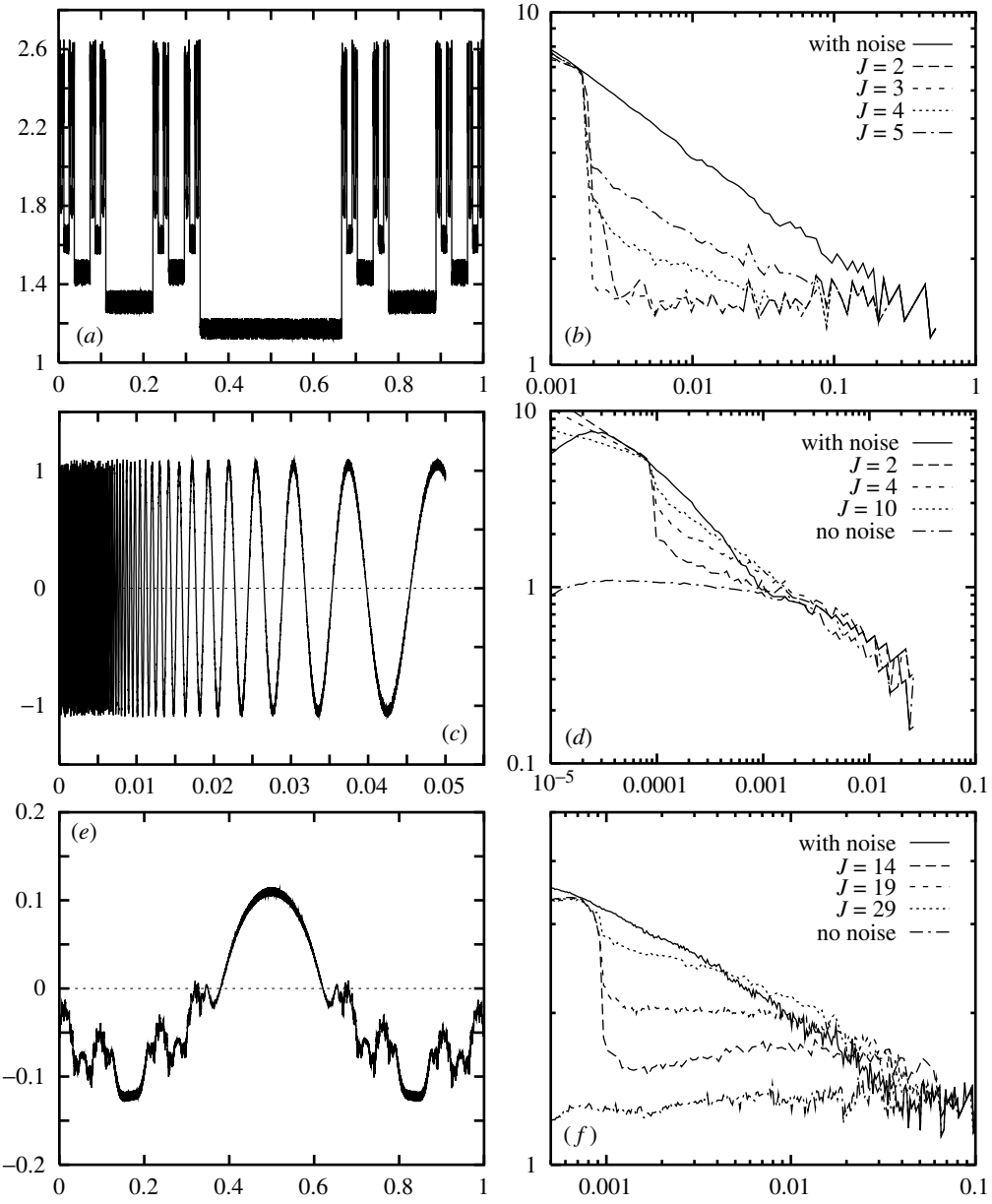

Figure 14. Control of the effect of noise on D_{E}.

and we can draw the same conclusion as with the signal of figure 14*a*, though here, $D_{\mathrm{E}} = 0.83$. For the signal in figure 14*c*, it turns out that D_{E}^{J} is not constant over an interval of J but we do observe, nevertheless, that $M_{\mathrm{E}}(r) \leqslant M_{\mathrm{E}}^{J}(r) \leqslant M_{\mathrm{E}}^{\mathrm{meas}}(r)$. In this case,

$$\frac{u_{\max} - u_{\min}}{u_{\max}\epsilon_{\max}} = 20,$$

and $D_{\mathrm{E}} = 0.3$. This analysis of these three topologically different intermittent sig-

Table 2. *Main characteristics of the two experimental signals from Modane*

figure	Re_λ	resolution	η (m)	η (s)	λ (m)	λ (s)	u' (ms^{-1})
12*a*	835	2η	1.40×10^{-4}	2.01×10^{-5}	7.8×10^{-3}	1.20×10^{-3}	1.65
12*b*	3050	1.2η	3.5×10^{-4}	1.75×10^{-5}	3.85×10^{-2}	1.93×10^{-3}	0.8

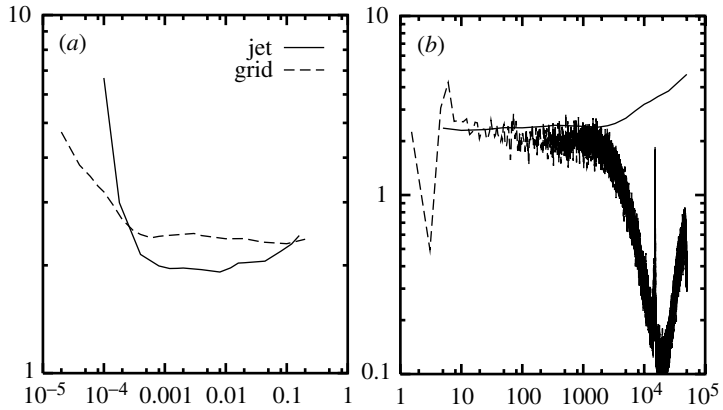

Figure 15. (*a*) $r^{0.11}F(r)$ as a function of r for jet and grid turbulence. (*b*) $k^{-5/3}E(k)$ (dashed line) compared with $r^{0.11}F(r)$ as a function of $1/r$ for case 12*b*.

nals with noise confirms our expectation that $D_{\mathrm{E}} \leqslant D_{\mathrm{E}}^{J} \leqslant D_{\mathrm{E}}^{\mathrm{meas}}$, and that our measurement of D_{E}^{J} on the basis of the intermediary signal $u^{J}(x)$ leads to significant improvement of the measurement of D_{E} by yielding an upper limit D_{E}^{J} less affected by the noise and smaller than $D_{\mathrm{E}}^{\mathrm{meas}}$.

We now apply this method to two high-resolution one-point turbulent velocity signals obtained by Y. Gagne and his team in Grenoble (see Arneodo *et al.* 1996). The first experimental signal was measured in a jet, its Reynolds number based on the Taylor microscale is $Re_\lambda = 835$ and its resolution is 2η, where η is the Kolmogorov length-scale. The second experimental signal was measured in a grid turbulence and has a higher Reynolds number ($Re_\lambda = 3050$) and a higher resolution (1.2η). These signals are referred to as 12*a* and 12*b* throughout this paper. Their main characteristics are given in table 2.

Figure 15*a* shows the curve $F(r)$ as a function of r for both signals. One can observe a range of scales where $F(r) \sim r^{-0.11}$. Figure 15*b* shows that $E(k) \sim k^{-5/3}$ ($E(k)$ is the energy spectrum and k the wavenumber) and $F(r) \sim r^{-0.11}$ are valid over the same range of scales. If an inertial range of scales exists, this range should be it, and we observe that it lies one or two decades above η for $Re_\lambda = 3050$.

We measure D_{E}^{J} for the two experimental signals in figure 12*a*, *b*, and assume that we can extend to these cases the result $D_{\mathrm{E}}^{J} < D_{\mathrm{E}}^{\mathrm{meas}}$. Supporting this assumption, we find that the eddy capacity D_{E}^{J} is independent of J in the range $3 < J < 9$. The value of D_{E}^{J} is the same for all values of J between 4 and 8, but this value is defined over a range of scales that grows as J increases from 4 to 8. When $J \geqslant 9$, the noise is abruptly retrieved, and $D_{\mathrm{E}}^{J} = 1 = D_{\mathrm{E}}^{\mathrm{meas}}$ over the entire range.

Figure 13*b* shows $r^{D_{\mathrm{E}}^{J}} M_{\mathrm{E}}^{J}(r)$ as a function of r in the cases of jet and grid turbulence; eddy capacities are clearly well defined over nearly two decades. The eddy

capacity measured as a least-squares value over this range of scales is 0.94 (± 0.01) for both jet and grid turbulence. $J = 8$ gives the smallest scale down to which we can measure D_{E}^{J}, and figure 13*b* shows that this inner scale is 1.6λ in the present datasets. This method gives no information about the dissipation range ($r \ll \lambda$).

It is interesting to note that D_{E}^{J} and q are well defined over approximately the same range of length-scales, and that, because $q \approx 0.11$ and $D_{\mathrm{E}}^{J} \approx 0.94$ for $3 < J < 9$, $q + D_{\mathrm{E}}^{J} \approx 1.05$ and

$$q + D_{\mathrm{E}} \leqslant 1.05$$

(to compare with (2.6)). Note also that D_{E} is clearly different from 1, and, therefore, neither the jet nor the grid turbulence can be modelled by signals such as that in figure 3, described in Benzi *et al.* (1993).

5. Conclusion

In this paper we have introduced a distinction between two topologically different types of intermittency: isolated and non-isolated.

Whereas the scalings of power spectra and second-order structure functions are influenced and sometimes even determined by the Kolmogorov capacity D'_{K} of the zero-crossings of the signal (Vassilicos & Hunt 1991; Hunt & Vassilicos 1991), the scalings of higher-order structure functions, and, in particular, that of the flatness factor, are often determined by the eddy capacity D_{E} of the signal, that is the Kolmogorov capacity of the zero-crossings of the second derivative of the signal. The capacities D_{E} and D'_{K} are, in general, different. *The eddy capacity is a direct measure of the geometry of intermittency.* Non-intermittent signals are such that $F(r) = \text{const.}$ and $D_{\mathrm{E}} = 1$, but the Kolmogorov capacity D'_{K} of their zero-crossings can take any value between 0 and 1; and if their power spectrum $E(k) \sim k^{-2p}$, then the power $2p$ is also insensitive to $D_{\mathrm{E}} = 1$, but is influenced and, in fact, often determined by D'_{K} (the relationships between D'_{K} and $2p$ are discussed in many of the references cited at the end of this paper). The eddy capacity of intermittent signals can, however, determine the scaling of the flatness factor, and we find that

$$F(r) \sim r^{-q}, \quad \text{with } q + D_{\mathrm{E}} = 1,$$

for a broad class of intermittent signals of both the isolated and the non-isolated topological types. The Kolmogorov capacity D'_{K} does not affect the scaling of the flatness factor except, of course, somehow indirectly, in the cases where $D'_{\mathrm{K}} = D_{\mathrm{E}}$. Examples where $D'_{\mathrm{K}} = D_{\mathrm{E}}$ are pictured in figure 4*a*, *b*, and examples where $D'_{\mathrm{K}} \neq D_{\mathrm{E}}$ are pictured in figures 1 and 7.

The results of our one-point turbulence data analysis indicate that inertial-range intermittency at high Reynolds numbers is such that $D_{\mathrm{E}} = 0.94$ and $F(r) \sim r^{-0.11}$ both for grid and jet turbulence. Inertial range turbulence is, therefore, intermittent, albeit weakly so, and signals such as those of figure 1 are, therefore, not good models of turbulence fluctuations. Furthermore,

$$q + D_{\mathrm{E}} \leqslant 1.05,$$

in the inertial range of high-Reynolds-number turbulence.

We are grateful to Yves Gagne for providing the turbulence datasets, and gratefully acknowledge financial support from the Royal Society and EPSRC grant GR/K50320.

Appendix A. D_{E} and D'_{K}

The eddy capacity D_{E} is a number between 0 and 1 and is a measure of how space filling eddies are in real space, whereas the Kolmogorov capacity D'_{K} of the zero-crossings of the signal $u(x)$ itself characterizes the distribution of energy among wavenumbers in Fourier space (Kevlahan & Vassilicos 1994). There is no general direct relation between D'_{K} and D_{E}. As can be seen from (2.4), D_{E} influences the scaling of moments of order $n > 2$. Instead, D'_{K} affects the scaling of *second*-order structure functions and power spectra. Indeed, the power spectrum $E(k)$ of self-similar signals $u(x)$ with a well-defined D'_{K} is given by (Vassilicos 1992),

$$E(k) \sim k^{-2+D'_{\mathrm{K}}-2\sigma}, \tag{A 1}$$

where σ is a scaling exponent characterizing local magnitudes of $u(x)$. For example, in the case of an on–off scalar field, such as may occur when the molecular diffusivity is very much smaller than the kinematic viscosity, $\sigma = 0$ (Vassilicos & Hunt 1991), and for signals $u(x) = x^s \sin x^{-t}$, $D'_{\mathrm{K}} = (t/(t+1))$ and (A 1) is valid with $\sigma = s(1-D'_{\mathrm{K}})$, provided that $-1 \leqslant 2s \leqslant t$ (see Kevlahan & Vassilicos 1994).

To summarize, the relevant geometrical scaling parameter for the description of intermittency is D_{E} and not D'_{K}; firstly, because $F(r) \sim r^{D_{\mathrm{E}}-1}$, whereas D'_{K} affects only second- and not higher-order structure functions; and, secondly, because, as shown by Kevlahan & Vassilicos (1994), D_{E} is a measure of how space filling eddies are in real space, whereas D'_{K} is a measure of how evenly or unevenly the energy is distributed among wavenumbers in Fourier space.

References

Arneodo, A. (and 23 others) 1996 Structure functions in turbulence, in various flow configurations, at Reynolds number between 30 and 5000, using extended self-similarity. *Europhys. Lett.* **34**, 411–416.

Batchelor, G. K. 1953 *The theory of homogeneous turbulence*. Cambridge University Press.

Batchelor, G. K. 1967 *An introduction to fluid dynamics*. Cambridge University Press.

Benzi, R., Biferale, L., Crisanti, A., Paladin, G., Vergassola, M. & Vulpiani, A. 1993 A random process for the construction of multiaffine fields. *Physica* D **65**, 352–358.

Falconer, K. 1990 *Fractal geometry mathematical foundations and applications*. Wiley.

Frisch, U. 1995 *Turbulence*. Cambridge University Press.

Hunt, J. C. R. & Vassilicos, J. C. 1991 Kolmogorov's contributions to the physical and geometrical understanding of small-scale turbulence and recent developments. *Proc. R. Soc. Lond.* A **434**, 183–210.

Kevlahan, N. K.-R. & Vassilicos, J. C. 1994 The space and scale dependencies of the self-similar structure of turbulence. *Proc. R. Soc. Lond.* A **447**, 341–363.

Lundgren 1982 Strained spiral vortex model for turbulent fine structures. *Phys. Fluids* **25**, 2193–2203.

Smith, L. A., Fournier, J.-D. & Spiegel, E. A. 1986 Lacunarity and intermittency in fluid turbulence. *Phys. Lett.* A **114**, 465–468.

Vassilicos, J. C. 1992 The multi-spiral model of turbulence and intermittency. In *Topological aspects of the dynamics of fluids and plasmas*, pp. 427–442. Kluwer.

Vassilicos, J. C. & Hunt, J. C. R. 1991 Fractal dimensions and spectra of interfaces with application to turbulence. *Proc. R. Soc. Lond.* A **435**, 505–534.